RSC Advances

PAPER

View Article Online
View Journal | View Issue

Cite this: *RSC Adv.*, 2019, **9**, 5756

Reusable bentonite clay: modelling and optimization of hazardous lead and *p*-nitrophenol adsorption using a response surface methodology approach

Mohamed Zbair, *[a] Zakaria Anfar [b] and Hassan Ait Ahsaine [b]

In this work, bentonite clay (BC) calcined at 500 °C was used as an adsorbent (BC-500) for the adsorption of Pb^{2+} and *p*-nitrophenol. The ability of BC-500 for the removal of Pb^{2+} and *p*-nitrophenol has been investigated. The adsorption studies tailored well the pseudo-first-order and the Langmuir model for Pb^{2+} and *p*-nitrophenol both. In addition, the optimal removal of Pb^{2+} and *p*-nitrophenol was found at pH 5 for Pb^{2+} and pH 6 for *p*-nitrophenol. However, the change of temperature (20–60 °C) was found to have a negative effect on the adsorption process on BC-500. Based on the Dubinin–Radushkevich model the adsorption occurs *via* a physical process. Accordingly, the adsorption mechanism was proposed using N_2-physisorption analysis before and after adsorption of Pb^{2+} and *p*-nitrophenol. The reusability of BC-500 was examined and the outcomes recommended that BC-500 had good potential as an economic and proficient adsorbent for Pb^{2+} or *p*-nitrophenol from contaminated water. Finally, the experimental Pb^{2+} and *p*-nitrophenol removal efficiency were found to be 90.93 ± 2.15% and 98.06 ± 1.87% while the predicted value by model equals 91.28 ± 1.68 and 97.24 ± 2.54, respectively, showing that the predicted model values are in good agreement with the experimental value.

Received 4th January 2019
Accepted 12th February 2019

DOI: 10.1039/c9ra00079h

rsc.li/rsc-advances

1. Introduction

At present, pollution caused by organic and inorganic compounds is a major problem for the world and is likely to cause health hazards, harm to ecology, damage to structures or amenities, and interference with the legitimate use of water.[1] Industries such as papermaking, electroplating, metal finishing, textiles, storage batteries, lead smelting, mining, plating, ceramics, leather, food, rubber, cosmetics, and plastics use different chemical compounds, which makes it possible to produce toxic effluents containing organic and inorganic contaminants.[2] Lead (Pb) is one of the most toxic elements, even at low concentrations, because of its presence in automobile fuel and the subsequent emission into the atmosphere in the exhaust gases.[3] Pb(II) metals affect the central nervous system, kidneys, liver, and gastrointestinal system, and may directly or indirectly cause diseases such as anemia, encephalopathy, hepatitis, and the nephrotic syndrome.[4] *p*-Nitrophenol is another toxic pollutant (found particularly in the effluents from pesticides, pharmaceuticals, petrochemicals, and other industries) with an impact on many organisms that live in aquatic ecosystems. The presence of *p*-nitrophenol and its analogues in the environment has become a great concern in recent years because of their increased discharge, toxic nature and adverse effects on the receiving water bodies.[5] Moreover, *p*-nitrophenol is responsible to cause degeneration in human proteins, tissue erosion, paralysis of the central nervous system, and damage to the liver, kidney and pancreas.[6] As a priority toxin (US Environmental Protection Agency) because of its potential harm on aquatic life, plants and human beings even at low concentrations. *p*-Nitrophenol is a common constituent of contaminated soil, ground water or leachate.[7,8] Hence, *p*-nitrophenol may cause severe environmental and public health problems, and it is mandatory to be treated before being discharged into the environment.

The wide usage of Pb(II) and *p*-nitrophenol in various industries have triggered the necessities of developing an efficient method to remove these pollutants from wastewaters.[9] The most common methods for removal of these pollutants from industrial effluents include chemical precipitation, oxidation, and ion exchanges and adsorption *etc.*[7,8,10] Adsorption process belongs to this category and it is found to be very effective and is applied in the liquid phase.[1,11–20] Many adsorbents have been tested on the adsorption of Pb^{2+} and *p*-nitrophenol. For instance, Tran *et al.*[11] have been reported 4.112 mmol g^{-1} of Pb^{2+} adsorption capacity using phenylalanine–Mg/AL(LDH). Yuanqing Huang *et al.*[21] have utilized a nitrilotriacetic acid anhydride modified ligno-cellulosic

[a]*Laboratory of Catalysis and Corrosion of Materials, Chouaïb Doukkali University, Faculty of Sciences El Jadida, BP. 20, El Jadida 24000, Morocco. E-mail: zbair.mohamed@gmail.com*

[b]*Materials and Environment Laboratory, Ibn Zohr University, Faculty of Sciences, Agadir, Morocco*

Table 1 Mathematical equations and models using in this study

Formula	Utility	Parameters	Ref.
$Q_{e,t} = \frac{(C_0 - C_{e,t}) \times V}{m}$	Adsorption capacity	C_0 (mg L^{-1}) and $C_{e,t}$ (mg L^{-1}) are the initial and equilibrium concentrations, respectively. m (g) is the weight of adsorbent and V (L) is the volume	38
$R\ (\%) = \left(\frac{C_0 - C_{e,t}}{C_0}\right) \times 100$	Removal efficiency		39
$Q_t = Q_{cal}(1 - \exp^{K_1 t})$	Pseudo-first-order	Q_e (mg g^{-1}) and Q_t (mg g^{-1}) are the adsorbed amounts at equilibrium and at times t (min), respectively. K_1 (min^{-1}): the rate constant; K_2 (g mg^{-1} min^{-1}): rate constant	40
$Q_t = \frac{(K_2 {Q_{cal}}^2 t)}{(1 + K_2 Q_{cal} t)}$	Pseudo-second-order		41
$Q_t = K_{ip} t^{\frac{1}{2}} + C$	Intraparticle diffusion	K_{ip} (mg g^{-1} $min^{-1/2}$): rate coefficient; C: thickness of the boundary layer	42
$Q_e = \frac{Q_m K_L C_e}{1 + K_L C_e}$	Langmuir isotherm	K_L: direct measure of the intensity of the adsorption process; Q_m: maximum adsorption capacity	43
$R_L = \frac{1}{1 + K_L C_0}$	Adsorption feasibility	The adsorption process can be de fined as irreversible ($R_L = 0$), favorable (R_L between 0 and 1), linear ($R_L = 1$) or unfavorable ($R_L < 1$)	44
$Q_e = K_f C_e^{\frac{1}{n}}$	Freundlich isotherm	K_F: adsorption capacity; n: adsorption behavior	45
$Q_e = Q_{DR} e^{(-K_{DR}\varepsilon^2)}$ $\varepsilon = RT \ln\left(1 + \frac{1}{C_e}\right)$ $E_{DR} = \sqrt{\frac{1}{2K_{DR}}}$	Dubinin–Radushkevich isotherm	Q_{DR} (mg g^{-1}) the theoretical adsorption capacity; K_{DR} (mol^2 kJ^{-2}) the constant related to adsorption energy and ε the Polanyi potential; E_{DR} (kJ mol^{-1}) is the mean free energy of adsorption	46–48
$\Delta G^\circ = -RT \ln K_c$ $\ln K_c = \frac{\Delta S^\circ}{R} - \frac{\Delta H^\circ}{RT}$	Gibbs free energy Van't Hoff	ΔG°: Gibbs free energy change; K_c: an equilibrium constant (dimensionless); R: gas constant; T: temperature ΔS°: entropy change; ΔH°: enthalpy change	49–51

material (NTAA-LCM) toward Pb^{2+} removal and indicated an adsorption capacity of 303.5 mg g^{-1} at 298 K. Also, Pb^{2+} was biosorbed using waste biomass (160 mg g^{-1} at 25 °C).[22] For *p*-nitrophenol removal, Q. Zhang *et al.*[23] have been found an adsorption capacity of 102 mg g^{-1} by ZnAl-layered double hydroxides. B. Liu *et al.*[24] reached a capacity of 11 mg g^{-1} by coal fly ash. Furthermore, Muthanna J. Ahmed *et al.*[25] have been utilized microporous activated carbon with an adsorption capacity of 185 mg g^{-1}.

In recent years, clays are alternative solutions for acting as activated carbon. Clays have been used for thousands of years and continue to be among the leading industrial material because they are natural, earthy and fine-grained material.[26] For a long time, clays have been also used for adsorption of various organic, inorganic substances due to its low cost and high removal efficiency (high surface area and exchange capacities).[10,27–31] However, on our knowledge there is lack of information on the adsorption of Pb(II) and *p*-nitrophenol especially on bentonite clay and the effect of some variables on its adsorption capacity, optimization using response surface methodology and regeneration. The Response Surface Methodology (RSM) is a collection of mathematical and statistical techniques useful for the modeling and analysis of problems in which response of interest is affected by several variables (Kumar *et al.*, 2017). Several published paper has been reported the utilization of RSM for the optimization and verification of scientific researches and industrial studies.[32–34]

In this research, bentonite clay (BC) from the region of Safi (Morocco) has been used as an adsorbent to remove Pb^{2+} and *p*-nitrophenol from aqueous solution. Adsorption experiments have been performed to look for equilibrium as well as adsorption kinetics. The experimental data were compared with by others studies and adsorption mechanism was proposed. RSM approach also was applied to determine the optimum removal efficiency and also to explain the relations between Pb^{2+} and *p*-nitrophenol removal and the pertinent parameters.

2. Experimental

2.1. Adsorbent's preparation

The adsorbent used in this study is the bentonite clay (BC) from the region of Safi (Morocco). The BC was primarily washed several times and then milled and sieved, acquiring the average diameter of 10 μm. The clay was subsequently calcined over 500 °C in a muffle for a period of 6 h. The calcination process is used in order to increase the adsorbent's stability. The obtained material was labeled: BC-500.

Table 2 Experimental levels for *p*-nitrophenol adsorption

Variable	Factor	Unit	$-1.68(\alpha)$	-1	0	1	$+1.68(\alpha)$
X_1	pH	—	2.63	4	6	8	9.36
X_2	Temperature	°C	11.59	15	20	25	28.40
X_3	Concentration	mg L^{-1}	39.90	44	50	56	60.09

Table 3 Experimental levels for lead adsorption

Variable	Factor	Unit	$-1.68(\alpha)$	-1	0	1	$+1.68(\alpha)$
X_1	pH	—	1.63	3	5	8	8.36
X_2	Temperature	°C	11.59	15	20	25	28.40
X_3	Concentration	mg L^{-1}	39.90	44	50	56	60.09

2.2. Characterization of adsorbent

BC-500 was analyzed using the X-ray diffraction (diffractometer Bruker D8 Advanced). Copper Kα radiation (λ = 1.5406 nm) produced at 50 kV and 20 mA. Infrared Spectra of BC-500 was recorded using Fourier Transform Spectrometer (Shimadzu FTIR-8400S) with a resolution of 4 cm^{-1} and 20 scans (400 to 4000 cm^{-1}). The surface area of BC-500 was determined using Micromeritics ASAP 2010. Scanning Electron Microscopy analysis was done using (Hitachi S2500, Japan). Scanning electron microscopy (SEM) analyses were performed using FEI, Quanta 200-ESEM operated at 20 kV. X-Ray fluorescence elemental analysis of BC-500 was done using Philips spectrophotometer equipment. The PZC (point zero charge) is the pH at which the surface has zero net charge; known as pH_{pzc} it is characteristic for amphoteric surfaces and affected by the type of surface sites and the structure. For the PZC determination 0.20 g of BC-20 were mixed with 50 mL of 0.01 M NaCl solution for 2 days. The starting solutions pH (2.0 to 12.0) was adjusted using HCl and NaOH. After 2 days, the final pH was measured. The point of zero charge of the AC-HP (pH_{pzc}) is the point where the curve pH_{final} *versus* $pH_{initial}$ crosses the line $pH_{initial} = pH_{final}$.[16,35–37]

2.3. Adsorbate

Stock solutions (1000 mg L^{-1}) of tested adsorbate were prepared by dissolving *p*-nitrophenol (Sigma-Aldrich) in double distilled water and Pb^{2+} was prepared by dissolving $Pb(NO_3)_2$ (Sigma-Aldrich) in 1% HNO_3 solution to avoid hydrolysis formation and precipitation. The working solution was prepared by diluting stock solution to appropriate volumes.

Table 4 Experimental results of lead and *p*-nitrophenol adsorption using CCD matrix

No. exp.	X_1	X_2	X_3	Lead adsorption removal%	*p*-Nitrophenol adsorption removal%
1	-1	-1	-1	32.52	48.23
2	1	-1	-1	80.54	72.71
3	-1	1	-1	43.30	51.21
4	1	1	-1	81.62	63.62
5	-1	-1	1	36.46	45.45
6	1	-1	1	67.50	66.60
7	-1	1	1	33.41	48.48
8	1	1	1	58.56	56.82
9	$-\alpha$	0	0	3.44	10.20
10	α	0	0	61.47	30.21
11	0	$-\alpha$	0	76.82	77.85
12	0	α	0	75.84	73.20
13	0	0	$-\alpha$	73.48	88.86
14	0	0	α	52.02	80.29
15	0	0	0	91.68	97.64
16	0	0	0	92.92	97.74
17	0	0	0	91.48	96.44

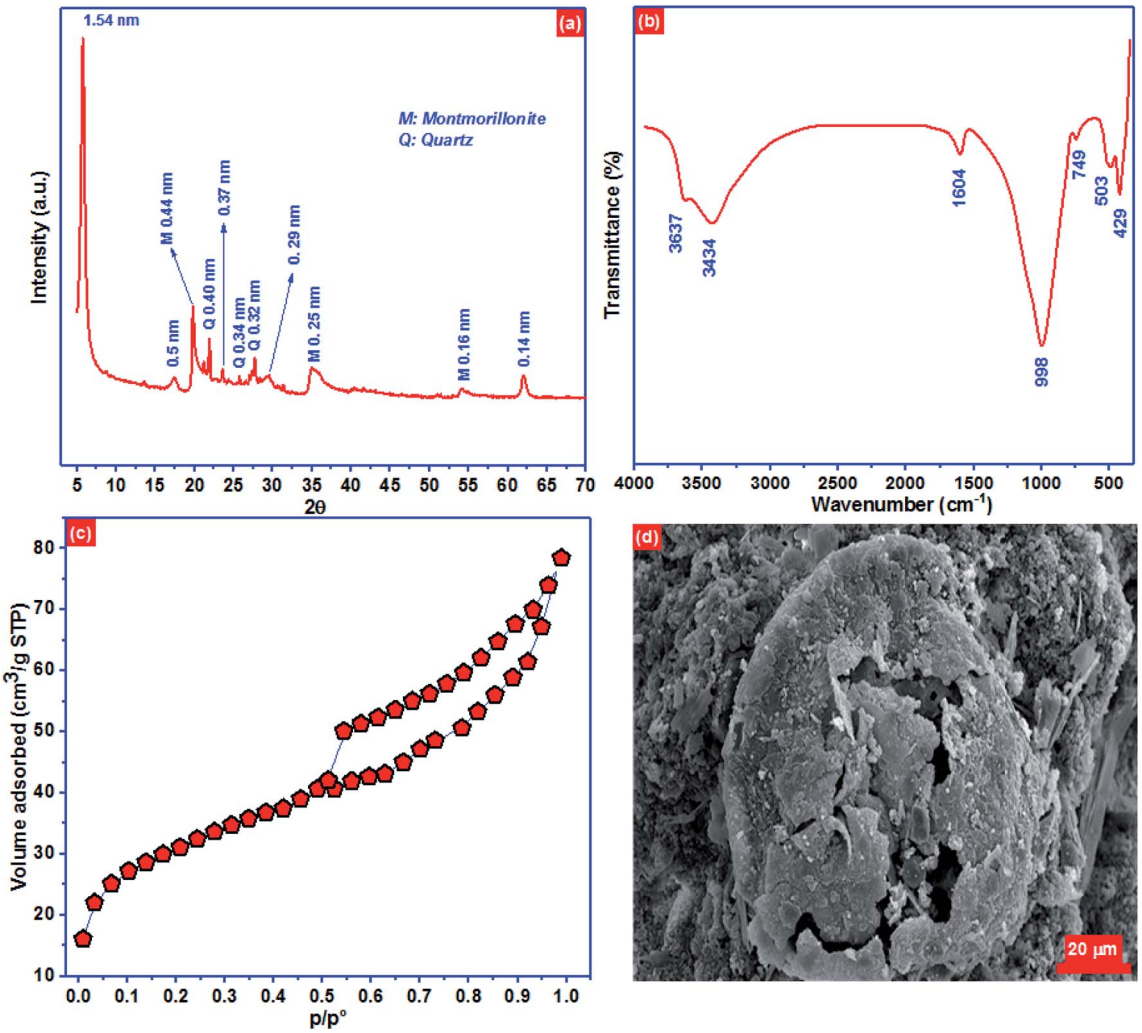

Fig. 1 (a) XRD pattern, (b) FTIR spectra, (c) N_2 physisorption isotherm and (d) the surface morphology of BC-500.

2.4. Adsorption experiments

Adsorption experiment was executed in duplicate, and the results were averaged. If the bias of the repeated experiment exceeded 15%, a triplicate run was performed.

The influence of the initial pH on adsorption of Pb^{2+} and *p*-nitrophenol onto BC-500 was observed by adjusting the pH value (2.0–12.0) at 20 °C by using 0.5 M HCl or 0.5 M NaOH prior to the experiments. Kinetics essays were carried out at three temperatures (20, 40, and 60 °C) in an Erlenmeyer by mixing 100 mg of BC-500 with 200 mL of Pb^{2+} and *p*-nitrophenol solution (concentration of 50 mg L^{-1}). The system was constantly shaken in order to keep the mixture's homogeneity and aliquots were collected at different time intervals (Pb^{2+}: 0–500 min and *p*-nitrophenol: 0–180 min). For adsorption equilibrium studies: various Pb^{2+} and *p*-nitrophenol solutions with different initial concentration at 20 °C (5–200 mg L^{-1} for Pb^{2+} and from 10–600 mg L^{-1} for *p*-nitrophenol). After the specified time, suspensions were filtered through filter paper Whatman 44. The concentration of the supernatant liquid of Pb^{2+} was determined by the absorption spectrophotometer AA-670. However, the concentration of *p*-nitrophenol was determined at $\lambda_{max} = 315$ nm using UV-Vis spectrophotometer spectrometry (Shimadzu-2600). Diverse theoretical kinetic and isotherm models are applied to experimental data in order to determine the best-fitting model Table 1.

2.5. Response surface methodology (RSM) technique

Among the methods used to optimize and modeling the adsorption process is the experimental methodology designs, more precisely the optimization by the RSM.[15] This method has attracted the attention of researchers in recent years.[32–34] Response surface methodology (RSM) was used to obtain optimum operational parameters.[52,53] The experimental levels

Table 5 Elementary chemical analysis by X-ray fluorescence

SiO_2	Al_2O_3	MgO	Na_2O	Fe_2O_3	TiO_2	CaO	K_2O	P_2O_5	LOI	Total
54.11	25.62	5.12	1.02	1.20	0.29	2.62	0.20	0.03	9.48	99.69

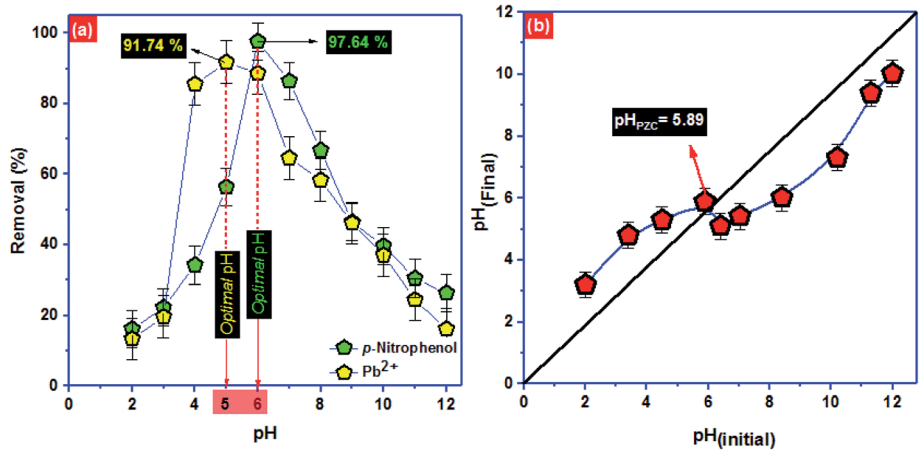

Fig. 2 (a) effect of pH solution and (b) the point of zero charge (pH_{pzc}) of BC-500.

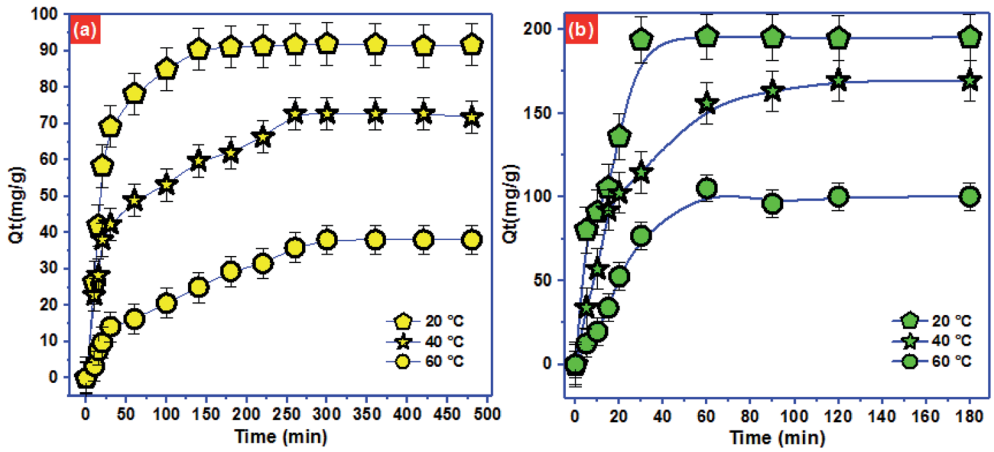

Fig. 3 Effect of contact time and temperature: (a): Pb(II); (b): *p*-nitrophenol.

Table 6 Different constants adsorption kinetics

		Pseudo-first-order				Pseudo-second-order		
		$Q_{e,exp}$ (mg g^{-1})	$Q_{e,cal}$ (mg g^{-1})	K_1 (min^{-1})	R^2	$Q_{e,cal}$ (mg g^{-1})	K_2 (g mg^{-1} min^{-1})	R^2
Pb^{2+}	20 °C	91.74	90.66 ± 1.07	0.043	0.988	97.96 ± 1.84	0.0006	0.980
	40 °C	71.74	75.09 ± 1.76	0.031	0.976	67.51 ± 7.12	0.0005	0.930
	60 °C	38.04	38.78 ± 1.45	0.008	0.982	47.90 ± 2.24	0.0002	0.973
p-Nitrophenol	20 °C	195.36	197.66 ± 7.29	0.066	0.961	219.13 ± 12.07	0.0004	0.948
	40 °C	169.71	168.08 ± 3.04	0.044	0.993	196.66 ± 5.86	0.0003	0.990
	60 °C	100.36	104.53 ± 5.18	0.034	0.993	128.18 ± 12.23	0.0003	0.939

		Intraparticle diffusion		
		K_{ip}	C	R^2
Pb^{2+}	20 °C	3.47	33.39 ± 8.19	0.705
	40 °C	2.99	18.48 ± 4.08	0.877
	60 °C	1.94	1.079 ± 1.36	0.861
p-Nitrophenol	20 °C	13.91	54.18 ± 21.22	0.740
	40 °C	13.44	24.10 ± 1.78	0.876
	60 °C	8.84	5.93 ± 1.42	0.828

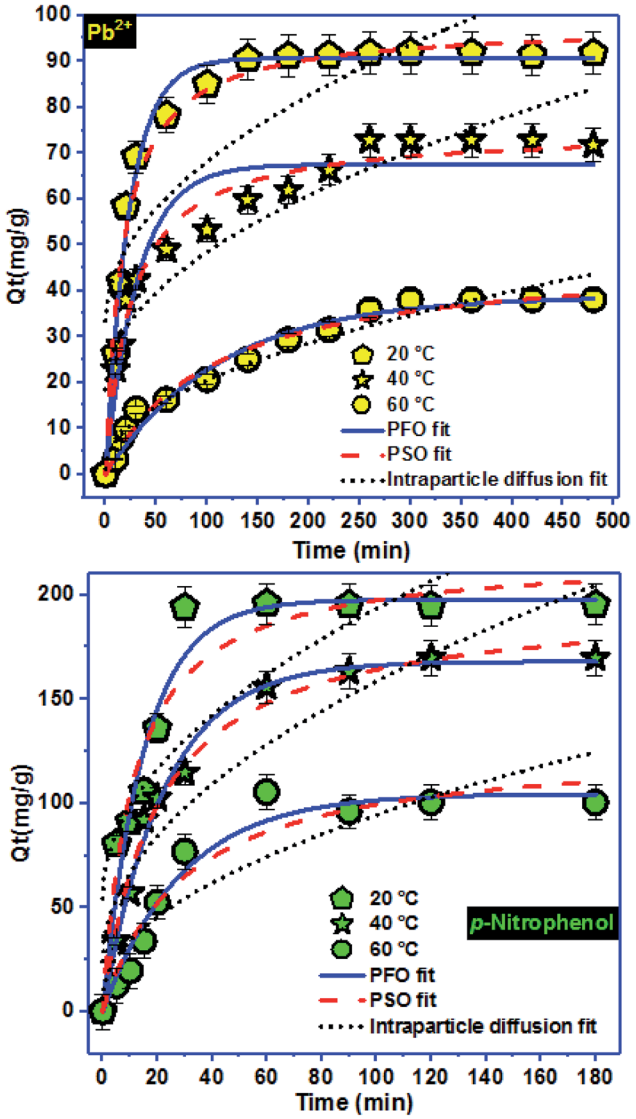

Fig. 4 Non-linear kinetics models adsorption of Pb^{2+} and *p*-nitrophenol onto BC-500.

for lead and *p*-nitrophenol adsorption were presented in Tables 2 and 3, respectively. The experimental results, as well as the CCD matrix, were shown in Table 4. Therefore, the quadratic polynomial equation that links the response lead and *p*-nitrophenol removal with three studied parameters were presented in equations below.

$$Y = b_0 + \sum_{i=1}^{k} b_i X_i + \sum_{i=1}^{k} b_{ii} X_1^2 + \sum_{i=1}^{k} b_{ij} X_i X_j$$

where Y is the predicted response lead or *p*-nitrophenol adsorption, b_0 is the intercept coefficient, b_i the linear terms, b_{ii} the squared terms, b_{ij} the interaction terms, and X_1, X_2 and X_3 represent the coded independent variables of pH, temperature and concentration, respectively.

3. Results and discussion

3.1. Characterization of BC-500

XRD pattern of the BC-500 exhibited mostly smectite described by the reflection of $d(001) = 1.54$ nm and minor impurities of quartz (Fig. 1a). Moreover, XRD of BC-500 presented the specific reflections consistent to d values of 1.54 nm (001), 0.50 nm (003), 0.37 nm (004) and 0.29 nm (005) for the basal values for smectites.[54] However, the reflexion of $d(003) = 0.44$ nm, $d(110) = 0.25$ nm, and $d(210) = 0.16$ nm is attributed to the presence of montmorillonite.[55,56] The reflection of $d(060) = 0.14$ nm is linked to a dioctahedral smectite in which the high intensity of d_{060} reflection designated a large size of the coherent domains along the b direction.[54,57]

FTIR spectra can reveal the surface functional groups on BC-500 surface qualitatively based on the typical absorbed energy for each bond in certain groups.[58] The surface functional groups in BC-500 are depicted in Fig. 1b. The peak located at 3637 cm^{-1} is ascribed to the groups stretching vibrations OH coordinated octahedral layer to Al(Mg)–O–H.[59,60] At 3434 cm^{-1} the peak corresponds to OH stretching of structural hydroxyl groups. The peak at 1604 cm^{-1} is associated with H–O–H deformation of water. However, the peaks observed at around 998 and 749 cm^{-1}

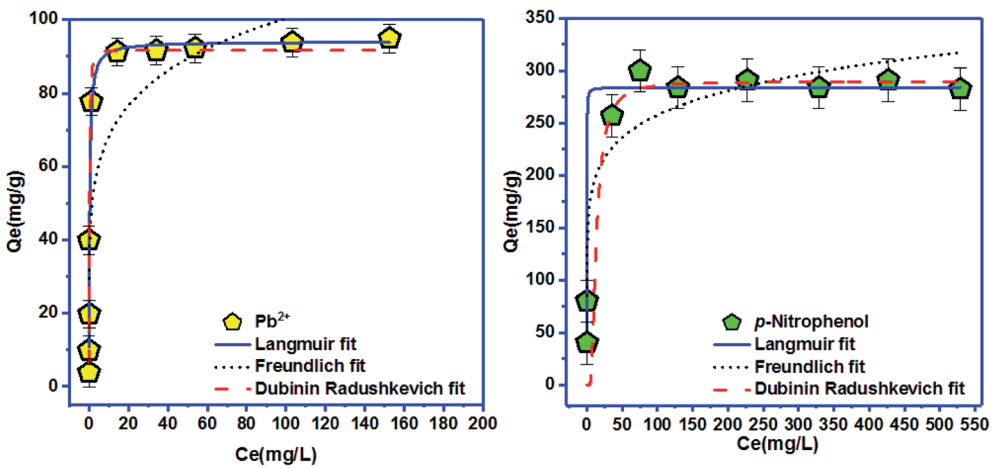

Fig. 5 Non-linear isotherms models used for adsorption of Pb^{2+} and *p*-nitrophenol onto BC-500.

Table 7 Isotherms parameters of Pb^{2+} and *p*-nitrophenol adsorption onto BC-500

	Langmuir isotherm				Freundlich isotherm		
	Q_{max} (mg g^{-1})	K_L (L mg^{-1})	R_L	R^2	K_F ((mg g^{-1}) (mg $L^{-1})^{-n}$)	n	R^2
Pb^{2+}	94.01	2.97	0.002	0.942	46.24	5.93	0.760
p-Nitrophenol	284.25	16.05	0.0001	0.971	145.01	8.01	0.886

	Dubinin–Radushkevich isotherm			
	Q_{DR} (mg g^{-1})	K_{DR} (mol^2 kJ^{-2})	R^2	E (kJ mol^{-1})
Pb^{2+}	91.63	0.260	0.928	1.386
p-Nitrophenol	289.82	138.74	0.910	0.060

Table 8 Comparison of the maximum adsorption capacity of BC-500 with other adsorbents

Adsorbent	Pb^{2+}	*p*-Nitrophenol	Ref.
BC-500	**94**	**284**	**This study**
Phaseolus hulls activated carbon	21	—	78
Ulva lactuca (AAC)	83	—	79
Apricot stone	23	—	80
Pecan shell	64	—	81
Nano illite/smectite clay	2	—	82
ZnAl-layered double hydroxides	—	102	23
Microporous activated carbon	—	185	25
Hypercrosslinked magnetic polymer	—	153	83
Coal fly ash	—	11	24
H_3PO_3-treated coal	—	256	84

are linked to Si–O–Si and Si–O stretching of silica and quartz.[61] The peaks at 503 and 429 cm^{-1} are assigned to Al–O–Si and Si–O deformation, respectively.[56]

Nitrogen physisorption isotherm of BC-500 presented in Fig. 1c, represent type IV adsorption isotherm with type H3 hysteresis loops which are characteristics of slit-like pore materials. The noticeable hysteresis loop can be seen on the BC-500 isotherm, signifying the existence of capillary condensation and the presence of mesopores. The BET surface area, total pore volume, and pore size of BC-500 are 101.2 m^2 g^{-1}, 0.26 cm^3 g^{-1}, and 4.8 nm, respectively. The surface morphology of BC-500 (Fig. 1d) shows porous and heterogeneous structures. This result is also in accord with the specific surface area of BC-500.

Elementary chemical analysis by X-ray fluorescence (Table 5) displays that Al_2O_3 and SiO_2 are the principal elements with a ratio of SiO_2/Al_2O_3 equal to 2.11. This value and the low content of K_2O (0.20%) designate that the BC-500 used in this work belongs to the family of smectite.[62] Moreover, the existence of exchangeable cations such as Ca^{2+}, Na^+, and Mg^{2+} indicates that the analyzed BC-500 has a high cation exchange capacity. These outcomes are entirely consistent with those stated by Er-ramly and Ider.[63]

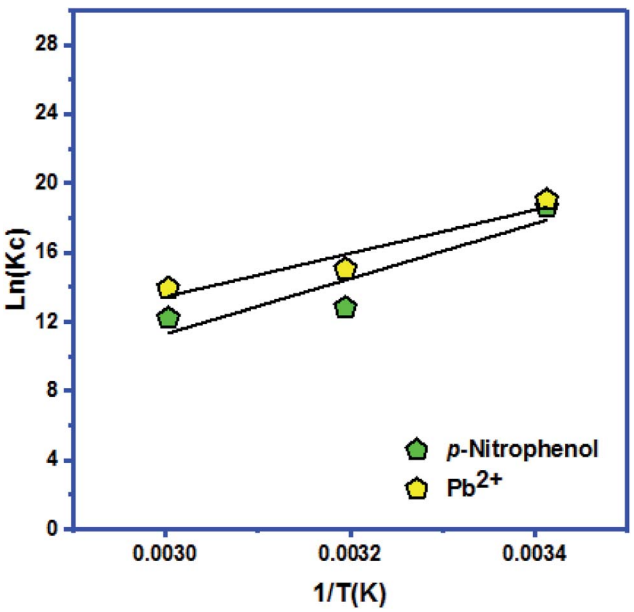

Fig. 6 Van't Hoff plot for Pb^{2+} and *p*-nitrophenol adsorption onto BC-500.

3.2. Adsorption of Pb^{2+} and *p*-nitrophenol

3.2.1. Effect of pH. It is well recognized that the pH of the adsorbate solution plays an essential role in the adsorption process.[64–66] For additional understanding, we conducted adsorption of Pb^{2+} and *p*-nitrophenol onto BC-500 at various pH values.

The removal efficiency increased from 13.4 to 91.74% for Pb^{2+} and 16.2–97.64% for *p*-nitrophenol by increasing the solution pH from 2.0 to 5.0 for Pb^{2+} and 2.0 to 6.0 for *p*-nitrophenol. However, the adsorption starts decreasing by 16.2 and 26.4% at pH 12.0 for Pb^{2+} and *p*-nitrophenol, respectively (Fig. 2a). The surface of the BC-500 has the point of zero charges (pH_{pzc}) at about 5.89 (Fig. 2b). The decrease in H_3O^+ with increasing pH in the acidic solution might increase the electrostatic attraction between the positively charged surface of the BC-500 and the partially negative charge of the *p*-nitrophenol

Table 9 Thermodynamic parameters for Pb^{2+} and *p*-nitrophenol adsorption onto BC-500

	ΔH (kJ mol^{-1})	ΔS (kJ mol^{-1} K^{-1})		ΔG (kJ mol^{-1}) 293 K	313 K	333 K
Ketoprofen	−104.499	−0.201	K_C	184 568 580	3 415 381.2	1 126 960.8
				−46.365	−39.148	−38.580
p-Nitrophenol	−132.467	−0.303	K_C	123 915 710.3	362 868.435	199 963.6695
				−463.657	−33.313	−33.792

molecules, consequently increasing the adsorption. The BC-500 surface starts to develop a partial negative charge at pH higher than pH_{pzc} (5.89) and the *p*-nitrophenol molecules exists as deprotonated from (*p*-nitrophenolate anion) at pH > pK_a = 7.15,[67] this forms an electrostatic repulsions between the negatively charges *p*-nitrophenol molecules and negative surface of BC-500, which is consistent with previous studies.[5,68,69]

At pH value between 2.0 to 4.0, the low removal of Pb^{2+} may be due to the competition with H^+ ions on active sites of BC-500. Furthermore, the decrease in the removal efficiency at pH values (6.0–12.0) might be linked to the formation of $Pb(OH)_2$ and an insoluble precipitate of Pb^{2+}.[70] In most of the stated studies regarding heavy metal ions adsorption onto various adsorbent, the adsorption removal displays a maximum for an initial pH at around 5.[70–74]

3.2.2. Effect of contact time and temperature. Contact time effect was performed in 200 mL of Pb^{2+} and *p*-nitrophenol solutions of 50 mg L^{-1} with varying contact time at optimal pH and three different temperatures (20, 40, and 60 °C). Fig. 3 displays the effect of different contact times on the adsorption of Pb^{2+} and *p*-nitrophenol on BC-500. The adsorption was rapid and approximately accomplished (adsorption equilibrium) in 140 min (Fig. 3a) and 30 min (Fig. 3b) at 20 °C for Pb^{2+} and *p*-nitrophenol, respectively. However, increasing temperature influence negatively on adsorption capacity from 92 to 38 mg g^{-1} in the case of Pb^{2+} and from 195 to 100 mg g^{-1} for *p*-nitrophenol, respectively. This might be related to desorption produced by an increase in the available thermal energy which modify the position of adsorption–desorption equilibrium.[66] This result shows that a low temperature favours the adsorption of for Pb^{2+} and *p*-nitrophenol on BC-500.

3.2.3. Adsorption kinetics. The adsorption kinetics of Pb^{2+} and *p*-nitrophenol onto BC-500 were also examined. Pseudo-first (PFO), second order (PSO), and intraparticle diffusion (IPD) models were employed to correlate the kinetics data (Table 6). Adsorption kinetics data on BC-500 along with the linked model by means of the PFO, PSO, and IPD models were presented in Fig. 4.

To approve the best model that describe the adsorption kinetics of Pb^{2+} and *p*-nitrophenol onto BC-500, we usually compare the value of correlation coefficients and standard error of estimate (SEE) allowing the correlation between experimental data and the model-predicted values. The nonlinear plots of Pb^{2+} and *p*-nitrophenol adsorption kinetics and the calculated kinetic parameters are given in Fig. 4 and Table 6. As can be seen, the correlation coefficients found from PFO model was higher compared with R^2 gotten from PSO model. Additionally, the SEE of PFO model was the lowest one compared to PSO model. Consequently, PFO model describe well the adsorption data of Pb^{2+} and *p*-nitrophenol onto BC-500 at all studied temperature. Besides, the experimental adsorption capacity of Pb^{2+} and *p*-nitrophenol onto BC-500 were very close to the calculated one by PFO model (Table 6).

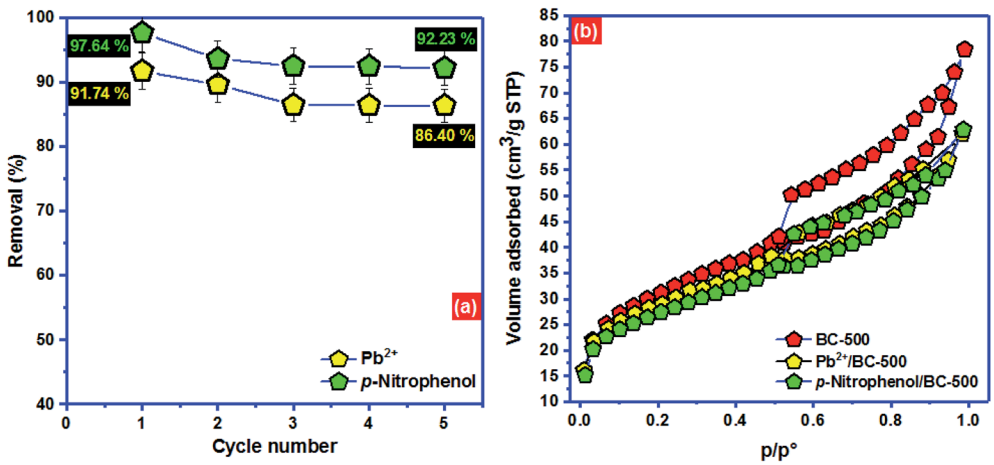

Fig. 7 (a) Regeneration of BC-500 and (b) adsorption mechanism of Pb^{2+} and *p*-nitrophenol onto BC-500.

Table 10 ANOVA analyses

NOM	Coefficient	*P*-value
Lead adsorption		
Model	—	<0.0001
b0	92.081	<0.0001
b1	17.583	<0.0001
b2	**−0.130**	**0.709**
b3	−5.722	<0.0001
b1-1	−21.246	<0.0001
b2-2	−5.733	<0.0001
b3-3	−10.535	<0.0001
b1-2	−1.949	0.00293
b1-3	−3.769	<0.0001
b2-3	−2.981	0.000248
Lack of fit		0.26
R^2	0.999	
$R_{Adj}{}^2$	0.998	
***p*-Nitrophenol adsorption**		
Model	—	<0.0001
b0	53.532	<0.0001
b1	17.249	<0.0001
b2	10.802	0.0200
b3	8.605	0.0206
b1-1	−2.998	<0.0001
b2-2	−2.689	<0.0001
b3-3	−4.416	<0.0001
b1-2	−0.720	0.0218
b1-3	**−2.542**	**0.2040**
b2-3	**−4.090**	**0.9070**
Lack of fit		0.104
R^2	0.997	
$R_{Adj}{}^2$	0.994	

In other hand, the increase in temperature decrease the acceleration of Pb^{2+} and *p*-nitrophenol adsorption on BC-500, which was certificated by the decrease in the second-order rate constants (K_2). This might be due to the increase of solution viscosity at high temperature and thus diminish the mass transfer and diffusion of the Pb^{2+} and *p*-nitrophenol inside BC-500.

Moreover, Fig. 4 displays the curve-fitting plots of IPD model for Pb^{2+} and *p*-nitrophenol onto BC-500 adsorption. The values of the intercept C of Pb^{2+} and *p*-nitrophenol give an idea about the boundary layer thickness: the larger intercept, the greater is the boundary layer effect in adsorption by BC-500. In the meantime, the plots do not pass over the origin, this specifies that there lies some degree of boundary layer control and the IPD is not the lonely rate-controlling step, but also other processes may control the rate of adsorption of Pb^{2+} and *p*-nitrophenol.[75] Hence, the IPD model is not appropriate for describing the Pb^{2+} and *p*-nitrophenol removal from water onto BC-500. It can be concluding that the PFO model described well the kinetics data of Pb^{2+} and *p*-nitrophenol compared to PFO and IPD models.

3.2.4. Adsorption isotherms. To investigate the most suitable correlation for the equilibrium data of Pb^{2+} and *p*-nitrophenol adsorption onto BC-500 (Fig. 5), three non-linear models were used, Langmuir, Freundlich, and Dubinin–Radushkevich (D–R). The calculated values for Langmuir, Freundlich, and Dubinin–Radushkevich parameters were summarized in Table 4. From Table 4, the adsorption of Pb^{2+} and *p*-nitrophenol onto BC-500 were well fitted to the Langmuir isotherm model with high R^2, which endorse the homogeneous distribution of active sites on the surface of BC-500.[4] In addition, the nature of the adsorption process on BC-500 was investigated by calculating the values of R_L and Freundlich constant *n*. As a result, the adsorption Pb^{2+} and *p*-nitrophenol onto BC-500 were favorable (R_L between 0 and 1, and $1/n$ parameter was smaller than 1).[17] Based on Langmuir isotherm (Table 7), the maximum adsorption capacities Q_{max} was equal 94.01 mg g^{-1} (for Pb^{2+} adsorption) and 284.25 mg g^{-1} (for *p*-nitrophenol adsorption).

To elucidate the physical and chemical adsorption nature of Pb^{2+} and *p*-nitrophenol onto BC-500, Langmuir and Freundlich isotherms are insufficient, for this purpose D–R isotherm is

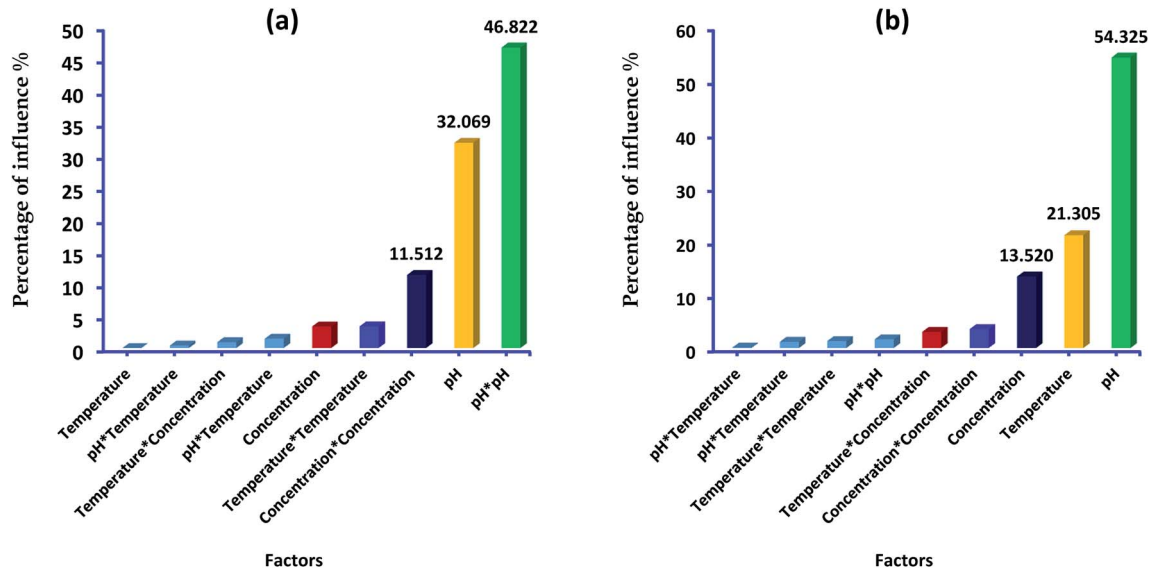

Fig. 8 Pareto chart for (a) lead and (b) *p*-nitrophenol adsorption.

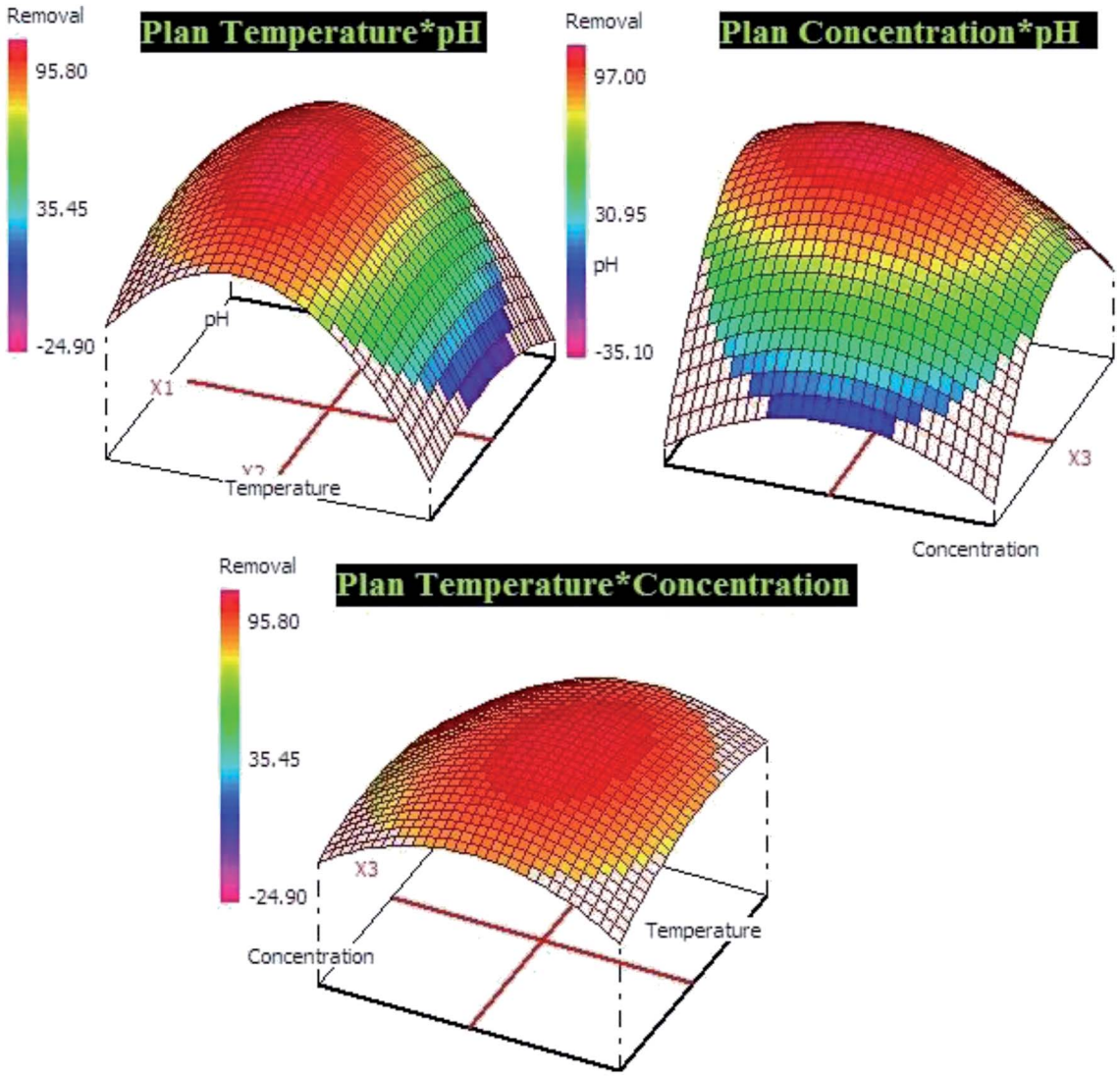

Fig. 9 RSM presentations for lead adsorption on different possible plans.

normally used.[30] The mean free energy of adsorption E_{DR} (E_{DR} of transference for 1 mol of solute from solution to the surface of CB-500 (ref. 76)), for Pb^{2+} and *p*-nitrophenol adsorption onto BC-500 was found equal to 1.386 kJ mol^{-1} (for Pb^{2+} adsorption) and 0.060 kJ mol^{-1} (for *p*-nitrophenol adsorption) (Table 7). These values are matching with other earlier studies using natural clay for adsorption in aqueous solutions.[30] Following the D–R isotherm model, $|E|$ values between 1–8 kJ mol^{-1} specify that the adsorption is a physical process, whereas, when $|E|$ are between 8.0 kJ mol^{-1} and 16 kJ mol^{-1} the adsorption occurs at an ion-exchange-type surface.[77] In our study, Pb^{2+} and *p*-nitrophenol adsorption onto BC-500, we found the values of E_{DR} is in the range of 1–8 kJ mol^{-1}, and consequently, mean that in our case the adsorption occurs *via* a physical process on BC-500. The adsorption capacity of BC-500 is compared to several adsorbents presented in Table 8. We found that the sorption capacity of BC-500 is better compared to others adsorbents.

3.2.5. Thermodynamic parameters. The comportment of adsorption (*i.e.*, physical or chemical) can be understood over the study of adsorption thermodynamics. The thermodynamic parameters (ΔG°, ΔH°, and ΔS°) can be calculated by the Van't Hoff approach.[50,85] The Van't Hoff equation and Gibbs energy equations (Table 9) were used to calculate the thermodynamic parameters of Pb^{2+} and *p*-nitrophenol adsorption on BC-500 (Fig. 6). From Table 9, the negative ΔG° values at all studied temperatures for Pb^{2+} and *p*-nitrophenol stipulate that the adsorption occurrence occurred spontaneously. Furthermore, the negative ($-\Delta S^\circ$) values disclose that the organization of Pb^{2+} and *p*-nitrophenol at the solid/solution interface through the adsorption process on BC-500 develops less random when the temperature increases. A negative value of ΔH° indicate that the adsorption process occurred exothermically. An exothermic process is obviously related to physical adsorption (physisorption) with the occurrence of relatively weak interactions (*i.e.*, van der Waals force).[86]

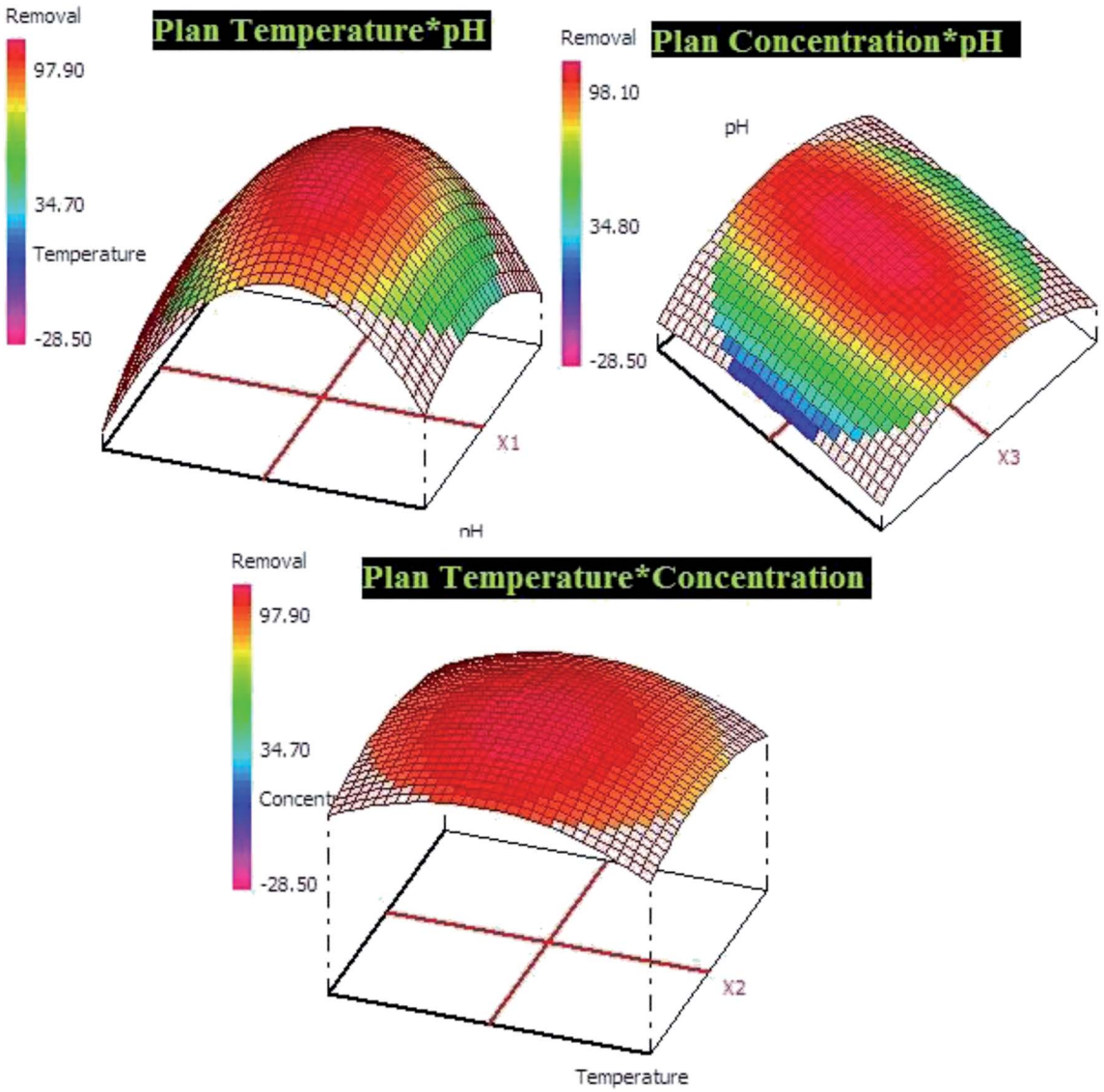

Fig. 10 RSM presentations for *p*-nitrophenol adsorption on different possible plans.

3.2.6. Regeneration of BC-500 and adsorption mechanism. Renewability is an essential concern to evaluate the adsorbent performance for wastewater treatment.[14,87] In order to distinguish the renewability of BC-500, the used BC-500 was washed out and then reused in the new experiments to evaluate its cycle performance. In this work, 0.5 M HCl and ethanol were used for Pb^{2+}/BC-500 and *p*-nitrophenol/BC-500 regeneration, respectively. The outcomes are illustrated in Fig. 7a. The Pb^{2+}/BC-500 regenerated by 0.5 M HCl revealed a slight decrease (−5.82%) from 91.74% to 86.40 after 5 cycles. Likewise, the *p*-nitrophenol/BC-500 regenerated by ethanol-exposed a small decreased (−5.54%). This suggests that BC-500 is an outstanding recycling adsorption material.

To advance the investigation of adsorption comportment of Pb^{2+} and *p*-nitrophenol onto BC-500, Fig. 7b displays the nitrogen physisorption isotherm for BC-500 before and after adsorption of Pb^{2+} and *p*-nitrophenol. After the adsorption of Pb^{2+} and *p*-nitrophenol onto BC-500, the surface area decreases noticeably from 101.2 to 94.4 $m^2\ g^{-1}$ and from 101.2 to 88.6 $m^2\ g^{-1}$, respectively. The total pore volume also diminishes from 0.26 to 0.19 $cm^3\ g^{-1}$ for Pb^{2+}/BC-500 and from 0.26 to 0.14 $cm^3\ g^{-1}$, which proves that the adsorbed Pb^{2+} and *p*-nitrophenol choose to be stored in the pores of BC-500 which is consistent with the outcomes of Dubinin–Radushkevich model.

3.2.7. Optimization of adsorption by response surface methodology (RSM). In this part of work, response surface methodology technique was used to optimize the adsorption process of Pb^{2+} and *p*-nitrophenol in order to modelled the reaction pathways taking into account the influence of different parameters as a function of lead and *p*-nitrophenol removal efficiency onto BC-500.[88,89] Therefore, the analysis of variance results (ANOVA) for lead or *p*-nitrophenol adsorption were presented in Table 10. Based on this statically analysis we conclude that:

Table 11 Experimental and predicted removal by the model for lead and *p*-nitrophenol adsorption

Adsorption of lead (pH = 5.0, temperature = 20.0 °C, concentration = 50.0 mg L^{-1})	
Predicted	Experimental
91.28 ± 1.68	90.93 ± 2.15
Adsorption of *p*-nitrophenol (pH = 6.0, temperature = 20.0 °C, concentration = 50.0 mg L^{-1})	
Predicted	Experimental
97.24 ± 2.54	98.06 ± 1.87

• The term '*P*-value' less than 0.05 implies that designed model is significant for both lead or *p*-nitrophenol.

• The correlation coefficient (R^2) and the adjusted correlation coefficient ($R_{Adj}{}^2$) prove the existence of a good correlation between data.

• The coefficients significations of models were studied at the 5% confidence level and their *P*-values less than 0.05, except b2 for lead adsorption and b2-1, b1-3 for *p*-nitrophenol adsorption.

In addition, Pareto diagram presented in Fig. 8 indicates that the parameters including square effect of pH, pH and square effect of concentration represent more than 90% of response variation in the case of lead adsorption. In the case of *p*-nitrophenol adsorption, pH, temperature and concentration influence the removal efficiency by 54.03%, 21.30% and 13.52, respectively. As results, Pareto analysis showed that the influence of pH was very high compared with other factors in both systems, which confirms the effect of electrostatic attractions mechanism during the adsorption of lead and *p*-nitrophenol.

The developed models for lead or *p*-nitrophenol adsorption were giving below using the quadratic polynomial equation.

$$R\%\ (\text{lead}) = 92.081 + 17.583X_{\text{pH}} - 5.722X_{\text{concentration}} - 21.246X_{\text{pH}} \times X_{\text{pH}} - 5.733X_{\text{Temperature}} \times X_{\text{Temperature}} - 10.535X_{\text{concentration}} \times X_{\text{concentration}} - 1.949X_{\text{pH}} \times X_{\text{concentration}} - 3.769X_{\text{pH}} \times X_{\text{concentration}} - 2.981X_{\text{concentration}} \times X_{\text{Temperature}}$$

$$R\%\ (p\text{-nitrophenol}) = 53.532 + 17.249X_{\text{pH}} + 10.802X_{\text{Temperature}} + 8.605X_{\text{concentration}} - 2.998X_{\text{pH}} \times X_{\text{pH}} - 2.689X_{\text{Temperature}} \times X_{\text{Temperature}} - 4.416X_{\text{concentration}} \times X_{\text{concentration}} - 0.720X_{\text{pH}} \times X_{\text{Temperature}} - 2.542XX_{\text{pH}} \times X_{\text{concentration}} - 4.090X_{\text{concentration}} \times X_{\text{Temperature}}$$

The both equations were used to elaborate the response surfaces which allows to obtain the optimization parameters of lead and *p*-nitrophenol adsorption and well understood the process (Fig. 9 and 10). Based on RSM presentation, the optimum conditions in term of lead and *p*-nitrophenol removal were showed in Table 11. Under these conditions the experimental and predicted removal by the obtained model showing a high correlation, which indicate the importance of this study in terms of modeling and optimization.

4. Conclusion

In this study, BC-500 as the low-cost adsorbent is talented to remove Pb^{2+} and *p*-nitrophenol from contaminated water very efficiently. The adsorption kinetic studies demonstrate that the removal of Pb^{2+} and *p*-nitrophenol is a rapid process and the adsorption process follows the pseudo-first-order model, demonstrating that Pb^{2+} and *p*-nitrophenol has a strong affinity on the BC-500 surface. It was found that the experimental isotherm data can be tailored well to the Langmuir equilibrium equation and BC-500 has very high Pb^{2+} and *p*-nitrophenol adsorption capacity of approximately 94 mg g^{-1} and 284 mg g^{-1} at 20 °C, respectively. Increasing temperature (20–60 °C) has an effect negative on adsorption capacity Pb^{2+} and *p*-nitrophenol. The removal of Pb^{2+} and *p*-nitrophenol depend clearly on the pH of the solution. The study on adsorption mechanism displays that the adsorption of Pb^{2+} and *p*-nitrophenol on BC-500 is dominated by physisorption process. Finally, the optimized parameters by the RSM method showed a good agreement between the predicted and experimental results.

Conflicts of interest

Authors declare that they have no conflict of interest.

Acknowledgements

This work was supported by the Ibn Zohr University, Faculty of Sciences-Morocco.

References

1 T. S. Anirudhan and M. Ramachandran, *J. Colloid Interface Sci.*, 2006, **299**, 116–124.
2 T. S. Anirudhan and M. Ramachandran, *Process Saf. Environ. Prot.*, 2015, **95**, 215–225.
3 A. H. Jawad, R. A. Rachid, M. A. M. Ishak and L. D. Wilson, *Desalin. Water Treat.*, 2016, **1**, 25194–25206.
4 L. Wang, J. Zhang, R. Zhao, Y. Li, C. Li and C. Zhang, *Bioresour. Technol.*, 2010, **101**, 5808–5814.
5 B. Zhang, F. Li, T. Wu, D. Sun and Y. Li, *Colloids Surf., A*, 2015, **464**, 78–88.
6 A. dos Santos, M. F. Viante, D. J. Pochapski, A. J. Downs and C. A. P. Almeida, *J. Hazard. Mater.*, 2018, **355**, 136–144.
7 S. Dutta, J. K. Basu and R. N. Ghar, *Sep. Purif. Technol.*, 2001, **21**, 227–235.
8 S. Haydar, M. A. Ferro-García, J. Rivera-Utrilla and J. P. Joly, *Carbon*, 2003, **41**, 387–395.
9 W. S. W. Ngah and S. Fatinathan, *J. Environ. Manage.*, 2010, **91**, 958–969.
10 S. S. Tahir and R. Naseem, *Sep. Purif. Technol.*, 2007, **53**, 312–321.
11 H. N. Tran, C.-C. Lin and H.-P. Chao, *Sep. Purif. Technol.*, 2018, **192**, 36–45.

12 H. J. He, Z. H. Xiang, X. J. Chen, H. Chen, H. Huang, M. Wen and C. P. Yang, *Int. J. Environ. Sci. Technol.*, 2018, **15**, 1491–1500.
13 M. Zbair, Z. Anfar, H. Khallok, H. A. Ahsaine, M. Ezahri and N. Elalem, *Fullerenes, Nanotubes, Carbon Nanostruct.*, 2018, **26**, 433–442.
14 Z. Anfar, M. Zbair, H. A. Ahsaine, M. Ezahri and N. El Alem, *Fullerenes, Nanotubes, Carbon Nanostruct.*, 2018, **26**, 389–397.
15 M. Zbair, Z. Anfar, H. A. Ahsaine, N. El Alem and M. Ezahri, *J. Environ. Manage.*, 2018, **206**, 383–397.
16 M. Zbair, H. A. Ahsaine and Z. Anfar, *J. Cleaner Prod.*, 2018, **202**, 571–581.
17 Z. Anfar, R. El Haouti, S. Lhanafi, M. Benafqir, Y. Azougarh and N. El Alem, *J. Environ. Chem. Eng.*, 2017, **5**, 5857–5867.
18 H. Ait Ahsaine, M. Zbair, Z. Anfar, Y. Naciri, R. El haouti, N. El Alem and M. Ezahri, *Mater. Today Chem.*, 2018, **8**, 1–12.
19 I. Anastopoulos, A. Bhatnagar, B. Hameed, Y. S. Ok and M. Omirou, *J. Mol. Liq.*, 2017, **240**, 179–188.
20 L. Bulgariu and D. Bulgariu, *J. Cleaner Prod.*, 2018, **197**, 875–885.
21 Y. Huang, C. Yang, Z. Sun, G. Zeng and H. He, *RSC Adv.*, 2015, **5**, 11475–11484.
22 C. Yan, Y. Chunping, H. Huijun, Z. Guangming, Z. Kun and Y. Zhou, *J. Environ. Eng.*, 2016, **142**, C4015001.
23 Q. Zhang, C. Peter Okoli, L. Wang and T. Liang, *Desalin. Water Treat.*, 2015, **55**, 1575–1585.
24 B. Liu, F. Yang, Y. Zou and Y. Peng, *J. Chem. Eng. Data*, 2014, **59**, 1476–1482.
25 M. Ahmed and S. Theydan, *Adsorptive removal of p-nitrophenol on microporous activated carbon by $FeCl_3$ activation: equilibrium and kinetics studies*, 2014, vol. 55.
26 A. Sari, M. Tuzen and M. Soylak, *J. Hazard. Mater.*, 2007, **144**, 41–46.
27 G. Bereket, A. Z. Aroğuz and M. Z. Özel, *J. Colloid Interface Sci.*, 1997, **187**, 338–343.
28 M. Tuzen, E. Melek and M. Soylak, *J. Hazard. Mater.*, 2006, **136**, 597–603.
29 N. L. D. Filho, W. L. Polito and Y. Gushikem, *Talanta*, 1995, **42**, 1031–1036.
30 S. Veli and B. Alyüz, *J. Hazard. Mater.*, 2007, **149**, 226–233.
31 S. S. Tahir and N. Rauf, *Chemosphere*, 2006, **63**, 1842–1848.
32 K. Zhao, Y. Cheng, H. Liu, C. Yang, L. Qiu, G. Zeng and H. He, *RSC Adv.*, 2015, **5**, 66013–66023.
33 L. Qiu, Y. Cheng, C. Yang, G. Zeng, Z. Long, S. Wei, K. Zhao and L. Luo, *RSC Adv.*, 2016, **6**, 17036–17045.
34 C. Yang, K. Zhao, Y. Cheng, G. Zeng, M. Zhang, J. Shao and L. Lu, *Sep. Purif. Technol.*, 2016, **163**, 153–161.
35 T. K. M. Prashantha Kumar, T. R. Mandlimath, P. Sangeetha, P. Sakthivel, S. K. Revathi, S. K. Ashok Kumar and S. K. Sahoo, *RSC Adv.*, 2015, **5**, 108034–108043.
36 D. Mohan, A. Sarswat, V. K. Singh, M. Alexandre-Franco and C. U. Pittman Jr, *Chem. Eng. J.*, 2011, **172**, 1111–1125.
37 J. S. Noh and J. A. Schwarz, *J. Colloid Interface Sci.*, 1989, **130**, 157–164.
38 J. Wang, C. P. Huang, H. E. Allen, D. K. Cha and D. W. Kim, *J. Colloid Interface Sci.*, 1998, **208**, 518–528.
39 V. K. Garg, R. Gupta, A. B. Yadav and R. Kumar, *Bioresour. Technol.*, 2003, **89**, 121–124.
40 S. Lagergren, *K. Sven. Vetenskapsakad. Handl.*, 1898, **24**, 1.
41 G. McKay, *Process Biochem.*, 1999, **34**, 451.
42 J. C. Weber and W. J. Morris, *J. Sanit. Eng. Div., Am. Soc. Civ. Eng.*, 1963, **89**, 31–60.
43 I. Langmuir, *J. Am. Chem. Soc.*, 1916, **38**, 2221–2295.
44 S. Fan, Y. Wang, Z. Wang, J. Tang, J. Tang and X. Li, *J. Environ. Chem. Eng.*, 2017, **5**, 601–611.
45 H. Freundlich, *Z. Phys. Chem.*, 1906, **57**, 385.
46 L. V. Dubinin and M. M. Radushkevich, *Proc. Acad. Sci. USSR, Phys. Chem. Sect.*, 1947, **55**, 331–333.
47 G. F. Cerofolini, *Surf. Sci.*, 1975, **51**, 333–335.
48 M. Ghasemi, M. Naushad, N. Ghasemi and Y. Khosravi-fard, *J. Ind. Eng. Chem.*, 2014, **20**, 2193–2199.
49 E. C. Lima, A. Hosseini-Bandegharaei, J. C. Moreno-Piraján and I. Anastopoulos, *J. Mol. Liq.*, 2019, **273**, 425–434.
50 I. Anastopoulos and G. Z. Kyzas, *J. Mol. Liq.*, 2016, **218**, 174–185.
51 P. S. Ghosal and A. K. Gupta, *J. Mol. Liq.*, 2017, **225**, 137–146.
52 Z. Anfar, M. Zbair, H. A. Ahsaine, M. Ezahri and N. E. Alem, *Fullerenes, Nanotubes, Carbon Nanostruct.*, 2018, **26**, 389–397.
53 M. Zbair, K. Ainassaari, Z. El Assal, S. Ojala, N. El Ouahedy, R. L. Keiski, M. Bensitel and R. Brahmi, *Environ. Sci. Pollut. Res.*, 2018, **25**, 35657–35671.
54 F. G. Alabarse, R. V. Conceição, N. M. Balzaretti, F. Schenato and A. M. Xavier, *Appl. Clay Sci.*, 2011, **51**, 202–208.
55 X. Wang, S. Lu, L. Chen, J. Li, S. Dai and X. Wang, *J. Radioanal. Nucl. Chem.*, 2015, **306**, 497–505.
56 M. El Miz, H. Akichoh, D. Berraaouan, S. Salhi and A. Tahani, *Am. J. Chem.*, 2017, **7**, 105–112.
57 L. M. Calarge, A. Meunier and M. L. L. Formoso, *J. South Am. Earth Sci.*, 2003, **16**, 187–198.
58 H. A. Ahsaine, M. Zbair and R. El Haouti, *Desalin. Water Treat.*, 2017, **85**, 330–338.
59 J. Madejová, W. P. Gates and S. Petit, in *Infrared and Raman Spectroscopies of Clay Minerals*, ed. W. P. Gates, J. T. Kloprogge, J. Madejová and F. Bergaya, Elsevier, 2017, vol. 8, pp. 107–149.
60 C. T. Johnston, in *Infrared and Raman Spectroscopies of Clay Minerals*, ed. W. P. Gates, J. T. Kloprogge, J. Madejová and F. Bergaya, Elsevier, 2017, vol. 8, pp. 288–309.
61 M. L. Cantuaria, A. F. de Almeida Neto, E. S. Nascimento and M. G. A. Vieira, *J. Cleaner Prod.*, 2016, **112**, 1112–1121.
62 L. Bounab, K. Draoui, M. Ahrouch, M. Hadri, D. Bouchta and A. Barhoun, *J. Mater. Environ. Sci.*, 2017, **8**, 244–256.
63 A. Er-ramly and A. Ider, *Phys. Chem. News*, 2011, **61**, 112–119.
64 H. N. Tran, C.-C. Lin, S. H. Woo and H.-P. Chao, *Appl. Clay Sci.*, 2018, **154**, 17–27.
65 I. Anastopoulos, I. Margiotoudis and I. Massas, *Int. J. Phytorem.*, 2018, **20**, 831–838.
66 M. Zbair, K. Ainassaari, A. Drif, S. Ojala, M. Bottlinger, M. Pirilä, R. L. Keiski, M. Bensitel and R. Brahmi, *Environ. Sci. Pollut. Res.*, 2018, **25**, 1869–1882.
67 D. Tang, Z. Zheng, K. Lin, J. Luan and J. Zhang, *J. Hazard. Mater.*, 2007, **143**, 49–56.

68 T.-H. Pham, B.-K. Lee and J. Kim, *Process Saf. Environ. Prot.*, 2016, **104**, 314–322.
69 G. Xue, M. Gao, Z. Gu, Z. Luo and Z. Hu, *Chem. Eng. J.*, 2013, **218**, 223–231.
70 M. Momčilović, M. Purenović, A. Bojić, A. Zarubica and M. Ranđelović, *Desalination*, 2011, **276**, 53–59.
71 A. Üçer, A. Uyanik and Ş. F. Aygün, *Sep. Purif. Technol.*, 2006, **47**, 113–118.
72 K. Kadirvelu, C. Faur-Brasquet and P. Le Cloirec, *Langmuir*, 2000, **16**, 8404–8409.
73 C. Faur-Brasquet, Z. Reddad, K. Kadirvelu and P. Le Cloirec, *Appl. Surf. Sci.*, 2002, **196**, 356–365.
74 S.-T. Lin, H. N. Tran, H.-P. Chao and J.-F. Lee, *Appl. Clay Sci.*, 2018, **162**, 443–453.
75 A. Sharma, Z. Syed, U. Brighu, A. B. Gupta and C. Ram, *J. Cleaner Prod.*, 2019, DOI: 10.1016/j.jclepro.2019.01.236.
76 F. Granados-Correa and J. Jiménez-Becerril, *J. Hazard. Mater.*, 2009, **162**, 1178–1184.
77 Y. Zeng, Z. Zeng, T. Ju and F. Zhang, *Microporous Mesoporous Mater.*, 2015, **210**, 60–68.
78 M. M. Rao, D. K. Ramana, K. Seshaiah, M. C. Wang and S. W. C. Chien, *J. Hazard. Mater.*, 2009, **166**, 1006–1013.
79 W. M. Ibrahim, A. F. Hassan and Y. A. Azab, *Egypt. J. Basic Appl. Sci.*, 2016, **3**, 241–249.
80 M. Kobya, E. Demirbas, E. Senturk and M. Ince, *Bioresour. Technol.*, 2005, **96**, 1518–1521.
81 R. R. Bansode, J. N. Losso, W. E. Marshall, R. M. Rao and R. J. Portier, *Bioresour. Technol.*, 2003, **89**, 115–119.
82 J. Yin, C. Deng, Z. Yu, X. Wang and G. Xu, *Water*, 2018, **10**, 210.
83 Y. Ma, Q. Zhou, A. Li, C. Shuang, Q. Shi and M. Zhang, *J. Hazard. Mater.*, 2014, **266**, 84–93.
84 S.-H. Lin and R.-S. Juang, *J. Environ. Manage.*, 2009, **90**, 1336–1349.
85 H. N. Tran, S. J. You, A. Hosseini-Bandegharaei and H. P. Chao, *Water Res.*, 2017, **120**, 88–116.
86 H. N. Tran, S.-J. You and H.-P. Chao, *J. Environ. Chem. Eng.*, 2016, **4**, 2671–2682.
87 A. Elouahli, M. Zbair, Z. Anfar, H. A. Ahsaine, H. Khallok, R. Chourak and Z. Hatim, *Surf. Interfaces*, 2018, **13**, 139–147.
88 H. Ait Ahsaine, Z. Anfar, M. Zbair, M. Ezahri and N. El Alem, *J. Chem.*, 2018, 1–14.
89 M. Zbair, Z. Anfar, H. A. Ahsaine and H. Khallok, *RSC Adv.*, 2019, **9**, 1084–1094.